Velocity characteristics of microwave-magnetic-envelope solitons

Hua Xia,* Pavel Kabos,† Reinhold A. Staudinger, and Carl E. Patton
Department of Physics, Colorado State University, Fort Collins, Colorado 80523

Andrei N. Slavin
Department of Physics, Oakland University, Rochester, Michigan 48309
(Received 20 January 1998)

The propagation properties of nonlinear microwave-magnetic-envelope (MME) wave packets, or MME solitons, have been measured as a function of input microwave power in a 7.56 μm-thick yttrium ion garnet film at 5 GHz with the static magnetic field of 1088 Oe parallel to the propagation direction in the backward volume wave configuration. Input pulse widths ranged from 13 to 38 ns. While linear MME wave packets at low power levels propagate at the usual group velocity v_g, the velocity of MME solitons increases with input power and shows characteristic plateaus at values given by $v_s^{(n)}=v_g+\kappa_n D$, where D is the dispersion coefficient and $\kappa_n=(2n-1)\pi/Tv_g$ is an effective wave-number parameter obtained from modulational instability considerations. The parameter $n=1$, 2, 3, etc., indexes the soliton order and T is the width of the input pulse. In between the plateau regions, the velocity increases more-or-less linearly with power, and the slope of the response generally increases with the initial pulse width T.
[S0163-1829(98)02029-3]

I. INTRODUCTION

The propagation properties of microwave-magnetic-envelope (MME) magnetostatic wave (MSW) packets change significantly at high power levels due to nonlinear effects. The main effect is the production of soliton wave packets with a characteristic steepening and narrowing, a nonlinear power response, a more rapid temporal and spatial decay than for linear MME pulses, and multiple peaks in the output profiles at very high powers. These MME soliton properties have been studied both experimentally and theoretically for yttrium iron garnet (YIG) films at frequencies in the GHZ range.[1–6]

One property of these MME pulses that has not yet been examined in a systematic way is the propagation velocity as a function of the various parameters of the experiment, such as input power and pulse width. It is known that velocity effects are small, no more than a few percent of the usual low power group velocity, and these effects were not considered in the references cited above. Moreover, theoretical analyses based on the nonlinear Schrödinger equation give no change in the wave packet velocity with increasing amplitude or power. In the course of the work reported in Ref. 6, however, small but systematic changes in the wave packet velocity as a function of input power were noted. The purpose of the present paper is to report on the further study of the velocity as a function of the input power, input pulse width, and propagation distance for these MME solitons. It is found that the velocity typically increases with the power and exhibits characteristic plateaus. These plateau levels match velocity values calculated from a simple *ad hoc* model based on modulational instability considerations. These effects are small, with velocity changes from the usual linear MSW group velocities on the order of a few percent. The quantitative determination and analysis of these effects required a careful and somewhat formal definition of velocity for wave packet shapes that may become distorted or modified during propagation.

II. EXPERIMENT

Background information on MSW pulse signal propagation in YIG films and measurement procedures is given in the references cited above. The measurements here were done according to the techniques given in Ref. 6. The MME pulses were excited through the application of microwave pulse power to a microstrip transducer across and close to one end of a long and narrow YIG film strip. The pulse power was supplied by a microwave synthesizer, a high-speed microwave switch, and a power amplifier. The power level was controlled by a variable attenuator. The static magnetic field was applied parallel to the long direction of the YIG film and the MSW pulse propagation direction. This arrangement corresponds to the magnetostatic backward volume wave (MSBVW) configuration. The microwave output signal or temporal profile for the propagated MSBVW pulse was detected by a second transducer placed across the YIG film strip at some distance away from the input transducer. The separation of the input and output transducer antenna could be varied in order to make time-of-flight measurements for different propagation distances. The input and output pulse signals were analyzed and stored through a microwave transition analyzer and a computer. Additional measurement were made with CW (continuous wave) microwave excitation in order to determine the MSBVW passband characteristics and establish an appropriate operating point in field and frequency. These details are discussed in Refs. 3 and 6.

The YIG film strip was the same as used for the work in Ref. 6. This film was provided by the Northrop-Grumman Science and Technology Center. The original film was grown on a (111) single-crystal gadolinium gallium garnet

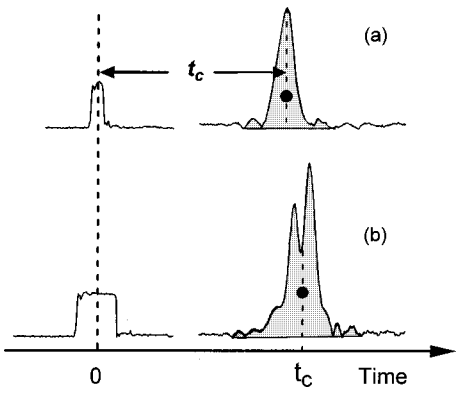

FIG. 1. Schematic diagram to illustrate the determination of the MSW pulse propagation time t_c. Diagram (a) shows the situation for a narrow input pulse centered at zero time and a symmetric output pulse with a peak at time t_c. Diagram (b) shows the situation for a wider input pulse and a highly structured output pulse for which the time t_c is defined from ''time-of-flight'' considerations, as discussed in the text.

substrate by liquid phase epitaxy. The film had a nominal thickness of 7.2 μm and a fitted thickness of 7.56 μm, as discussed in Ref. 6. The strip used for these experiments was 1.5 mm wide and 15 mm long. The input end of the strip was tapered to minimize reflections.

The transducer structure consisted of one fixed and one movable 50 μm-wide microstrip transducer. These transducer lines were positioned across the film and held firmly against the film surface. The input transducer was positioned about 4 mm from the tapered end of the film. The movable output transducer was positioned down the film at distances from 3 to 8 mm from the input line.

An operating point frequency of 5 GHz was chosen for the velocity experiments. The value of the external static magnetic field was then set by monitoring the MSBVW pass band of CW transmitted power vs frequency for the above MSBVW configuration. A field value of 1088 Oe yielded a pass band with an upper cutoff frequency point of 5.06 GHz. This arrangement positioned the 5 GHz operating point 60 MHz below the cutoff and yielded an acceptable transmission loss of about 20 dB. The calculated operating point MSBVW carrier wave number under these conditions was about 100 rad/cm. The input microwave pulse widths for the velocity measurements reported here were from 13 to 38 ns. The 13 ns width corresponds to a frequency spread of approximately ± 40 MHz, so that the entire power spectrum of the signal is within the MSBVW pass band.

This paper is concerned with precision measurements of the velocity of MME soliton pulses. As is evident from many of the references cited above and the data to follow, the actual waveform of the detected pulses can become complicated, particularly at high powers. It is necessary, therefore, to pay particular attention to the way in which the propagation time for the MME pulse from input to output is determined.

Figure 1 shows, in schematic form, the kind of situation that is encountered experimentally. The diagrams show profiles of power vs time for typical input and output pulses under different conditions. The upper trace in (a) shows a typical situation when the input pulse width is relatively narrow and the lower trace in (b) is for a wider input pulse.

For case (a), the output pulse is symmetric and shows a single, well-defined peak. In this case, the propagation time is easily defined as, for example, the separation in time between the input and output pulse center points. This time is indicated in the diagram as t_c. For initial pulse widths below 20 ns or so and peak powers below about 0.5 W, relatively uncomplicated pulse shapes of this sort were obtained. In these situations, a relatively simple procedure could be used to determine pulse propagating times. (1) The exact center point for a given output pulse was determined by fitting the measured profile to a hyperbolic secant function. (2) The peak position in time for the fitted function, relative to center of the input pulse, was then taken as the time t_c.

As shown in (b), the situation can be more complicated when the pulse width is increased. The output pulse in (b) shows two peaks and significant distortion. This situation can occur in soliton experiments when the input power is large, the input pulse width is large, and for various combinations of these conditions. Such complicated output pulse shapes present a problem for precision velocity measurements. While the separation of the input and output transducers is a well-defined parameter, how can one define the propagation time t_c in this case?

The solid circle that decorates the output pulse in diagram (b) of Fig. 1 is intended to indicate the ''time of flight'' of the pulse. For the purposes of this work, an operational definition of the propagation time t_c has been adopted, based on this ''time-of-flight'' idea. In analytical form, t_c is taken as the ''time of flight'' and written according to

$$t_c = \frac{\int |U(L,t)| t \, dt}{\int |U(L,t)| dt} . \tag{1}$$

The $U(L,t)$ function denotes the measured microwave output pulse profile, L is the transducer separation, and t represents the time of the measurement relative to the center of the input pulse. For the results reported below, U has been taken as the detected voltage due to the microwave output signal. One could also use the detected microwave power as the profile function in the evaluation of Eq. (1). These two approaches, however, yield differences in the determined t_c values of a few tenths of a nanosecond only.

Propagation times measured according to the procedure given above were measured for input pulse widths from 10 to 40 ns, input peak powers from 5 mW to 1.2 W, and transducer separation from 3 to 8 mm. This range of control parameters yields output signals that range from linear MSBVW pulse signals to nonlinear MME pulses in the order one to order three soliton regime.[3–5] Pulse widths greater than 40 ns yielded extremely complicated output pulse profiles. For such very wide pulses, meaningful determinations of pulse propagation times as well as the soliton formation were not possible. Results are shown below based on data for input pulse widths of 13, 25, and 38 ns.

The above data were used to obtain velocity values for the various combinations of experimental parameters listed above, based on an operational definition of velocity according to $\nu_c = L/t_c$. At low power levels, all ν_c determinations led to a common value, 3.51×10^6 cm/s. This value will be taken as the usual MSBVW linear excitation group velocity

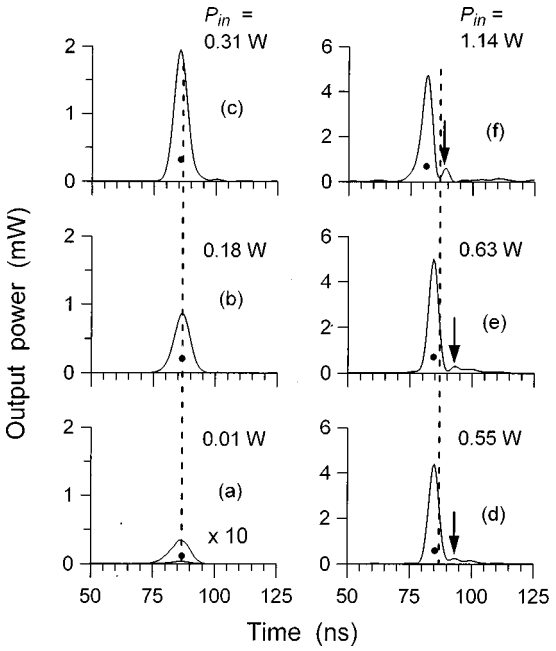

FIG. 2. Profiles of output power vs time for 13 ns-wide input pulses and input peak power P_{in} values as indicated. The carrier frequency, static field, and transducer separation were 5 GHz, 1088 Oe, and 3 mm, respectively, with the 7.2 μm nominal thickness YIG film in the MSBVW configuration. The solid circles show the time-of-flight position of the profiles or propagation time, as discussed in the text. The vertical dashed lines show the time-of-flight position for the lowest power in (a) on all the diagrams. The arrows in (d), (e), and (f) indicate the additional peak that emerges at high power.

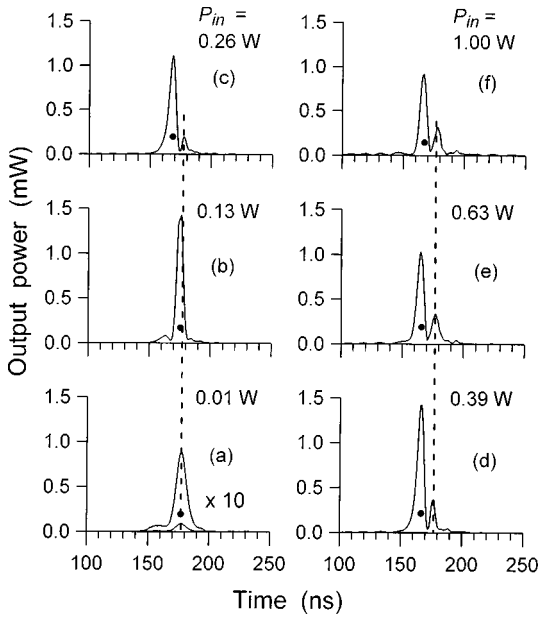

FIG. 3. Profiles of output power vs time for 25 ns-wide input pulses and input peak power P_{in} values as indicated. The transducer separation was 6.1 mm. Other conditions were the same as for Fig. 2. The solid circles show the time-of-flight positions and the vertical dashed lines show the time-of-flight position for the lowest power in (a) on all the diagrams, as in Fig. 2.

v_g. It was found that v_c typically increases slightly as the input power is increased, with changes on the order of a few percent for the range of powers available for the measurements. As will be shown in the next section, these increases, *albeit* small, show correlations with input power and pulse width that reveal important soliton effects.

Propagation time data and velocity determinations were also obtained as a function of the operating point carrier frequency at low power levels. These measurements were needed to determine the dispersion coefficient D for the MSBVW excitations at the 1088 Oe, 5 GHz operating point indicated above. The procedure is described in Ref. 6. The D parameter corresponds to the second derivative of the MSBVW angular frequency with respect to the wave number. This parameter was determined to be 1.36×10^3 cm^2/rad s.

III. RESULTS

A. Output profiles

Some typical output pulse profile measurement results are shown in Figs. 2–4. Each figure shows a sequence of six profiles of output power vs time for increasing values of the input pulse peak power level P_{in}, as indicated. The transducer separations were 3 mm for the Fig. 2 data and 6.1 mm for the Fig. 3 and Fig. 4 data. The input pulse widths were 13, 25, and 38 ns, for Figs. 1, 2, and 3, respectively. The solid circles in each diagram indicates the time-of-flight point for the profile as discussed above. The vertical dashed lines in the diagrams for each figure show the output pulse time-of-flight position at the lowest power, and matchup with the solid circles for the (a) diagrams in each figure. These circles and dashed lines provide reference points to understand the effect of power on propagation time. Because of the very low power levels used for the (a) diagrams, these

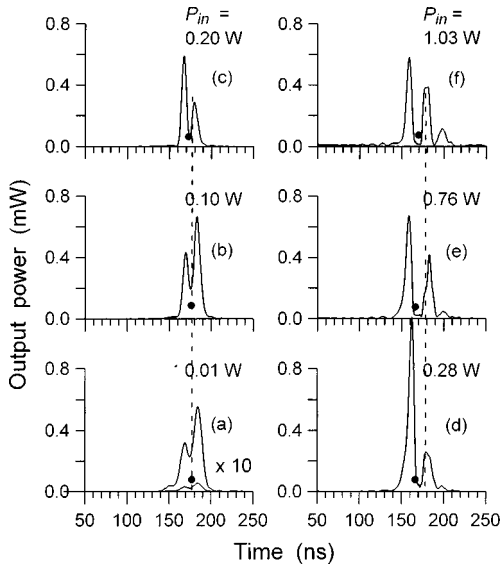

FIG. 4. Profiles of output power vs time for 38 ns-wide input pulses and input peak power P_{in} values as indicated. The transducer separation was 6.1 mm. Other conditions were the same as for Fig. 3. The solid circles show the time-of-flight positions and the vertical dashed lines show the time-of-flight position for the lowest power in (a) on all the diagrams, as in Fig. 2.

profiles have been magnified by a factor of ten, as indicated. The arrows in (d)–(f) of Fig. 2 indicate the additional peak that emerges at high power.

Figures 2–4 demonstrate common features that reflect the change in soliton velocity with power and special features that demonstrate the effect of the input pulse width on the pulse structure and evolution in the soliton order. As the later discussion will show, these features are tied together in a consistent way.

Consider first the common features. Note that each set of diagrams shows a decrease in the time-of-flight point with increasing power. This is shown by the gradual downshift of the solid circles relative to the vertical dashed lines from the (a) diagrams to the (d) diagrams in each figure. The size of these shifts is about 6–7 ns for Fig. 2, compared to the total propagation time at low power of about 87 ns. For Figs. 3 and 4, the shifts are about 5 ns, compared to a propagation time of about 177 ns. These shifts correspond to velocity changes of 3–7%. It is now clear why it is necessary to pay careful attention to the definition of the propagation time. More casual definitions, based on peak positions, for example, would result in effects that obscure the small changes evident from the time-of-flight points. In the case of the multipeaked profiles in Figs. 4 and 5, peak positions would provide no useful timing points whatsoever.

The actual velocities evident from the above data will be important for the analysis to follow. The diagram (a) data for Fig. 2 give a velocity at low power of about 3.5×10^6 cm/s. For Figs. 3 and 4, the lower power velocity is about 3.4×10^6 cm/s.

Now consider the different features for Figs. 2–4. Figure 2 is for a relatively narrow input pulse width of 13 ns. In this case, all of the output profiles exhibit a single peak only, apart for a very small secondary peak at high powers that will be considered shortly. For the two lowest input power levels of 0.01 and 0.18 W, as for (a) and (b), the output peak power scales more or less with the input power $P_{\rm in}$ and there is no downshift in the peak time-of-flight position. As the power is increased further, however, the output pulse show a consistent downshift in the time-of-flight position. For (d), and an input peak power of 0.55 W, the downshift amounts to about 6–7 ns. These downshifts in the time-of-flight position for diagrams (c) through (f) are accompanied by the steepening and narrowing usually associated with MME solitons.[1,3] As will be evident shortly, these downshifts correspond to an increase in MME pulse velocity that is almost linear in input power and closely matches the changes expected for solitons.

The additional feature of the data in Fig. 2 is the small secondary peak that comes in at the highest powers, as indicated by the arrow in diagrams (d)–(f). This small peak evolves from the tail-like traces in (d) and (e) to the small peak evident in (f). For the range of powers available, up to 1.2 W, this secondary peak is unable to develop significantly for the 13 ns input pulse width used here. This situation will be different for wider input pulses and the Fig. 3 and Fig. 4 data considered below.

If the input pulse width is wider than the 13 ns value used for Fig. 2, the output pulses show a much more complicated behavior. The data in Figs. 3 and 4 for input pulse widths of 25 and 38 ns, respectively, illustrates these changes. The main feature of note from all the diagrams in both figures is the multipeaked nature of the output profiles. Diagram (a) in Fig. 3, for example, shows an initial output profile at the lowest input power with a small, poorly resolved, peak for times just before the main peak. As the power is increased, this small peak becomes better resolved and shifts to times after the main peak. At the highest powers shown in Fig. 3, one clearly has a two peak output profile and a peak output power vs input power response that is highly nonlinear.

Similar comments apply to the 38 ns input pulse width data in Fig. 4. Here the evolution is even more accentuated. Initially, the rather pronounced secondary peak is below the main peak but is well resolved even at the lowest power. For input powers above 0.10 W, this peak moves above the main peak. For diagrams (d) and (e), the main peak decreases in amplitude as the power is increased, the secondary peak grows somewhat, and a *third* peak emerges at larger times.

The consistent drop in the peak power for the main peak as the input power is increased for diagrams (d)–(f) in both figures, the concurrent growth in the secondary peaks, and the emergence of the third peak for Fig. 4 suggest that the increased power is going more and more into these higher-order peaks. This kind of behavior is, in fact, one signature of a multisoliton response. The velocity data to be considered shortly, and the analysis of these data in Sec. IV, will demonstrate these multisoliton effects quite clearly.

The time-of-flight points in Figs. 3 and 4 show an additional effect that will be important for the multisoliton response analysis. If one notes the relative positions of the solid circles and the vertical dashed lines as one moves from (a) to (f) in each figure, it is seen that the downshift in the solid circle time-of-flight point *stabilizes* at high power. That is, the shift in the time-of-flight point relative to the propagation time at low power approaches a constant value. In terms of velocity, this means that the soliton velocity *saturates* at high powers. This will also turn out to be an important multisoliton signature.

B. MME pulse velocity

The pulse profile data in Figs. 2–4 allow one to obtain accurate values of the relevant velocities for the MME pulses discussed above. As specified in Sec.II, these velocities are obtained as L/t_c, where the propagation time t_c is the time-of-flight point defined by Eq. (1). As noted above, narrow pulses yield t_c values that match the time points obtained by hyperbolic secant line shape fitting procedures to better than 0.2 ns. For broader and more complicated output profiles, only the time-of-flight approach can yield consistent time points for velocity determinations.

Figures 5 and 6 show representative results on pulse velocity vs input peak power. The solid circles show measured velocities based on the time-of-flight values discussed above. The horizontal dashed lines show special velocity values corresponding to the low power group velocity v_g, and different order soliton limit velocities, as indicated. The labels $n=1$, $n=2$, and $n=3$ correspond to solitons of order n, as will be discussed in the next section. The carrier frequency and field conditions were the same as for Figs. 2–4; 5 GHz and 1088 Oe, respectively. Figure 5 shows one set of measurements for a single input pulse width of 13 ns and a 3 mm transducer

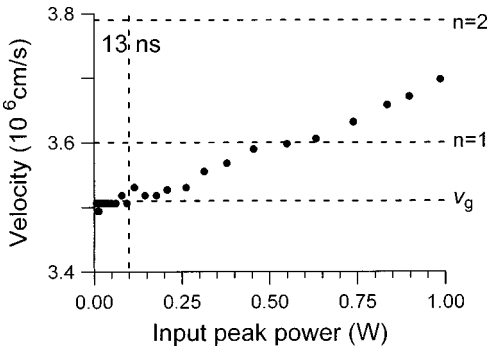

FIG. 5. Propagation velocity vs input peak power for MSBVW pulses propagated in the 7.56 μm-thick YIG film at a carrier frequency of 5.00 GHz. The input pulse width was 13 ns and the transducer separation was 3 mm. The static magnetic field parallel to the propagation direction was 1088 Oe. The horizontal dashed lines denote special velocities, as indicated. The vertical dashed line denotes the estimated threshold velocity for a nonlinear response.

separation. Figure 6 shows three sets of data for different pulse widths of (a) 13 ns, (b) 25 ns, and (c) 38 ns. The transducer spacing was kept at 6.1 mm for the Fig. 6 data. The vertical dashed line in Fig. 6 indicates an approximate power threshold for the increase in pulse velocity.

Figure 5 and graph (a) in Fig. 6 show a velocity that is essentially constant below a power of about 0.10 W and increases in a more or less linear fashion for higher powers. Note that the transducer separation of 6.1 mm for Fig. 6(a) is

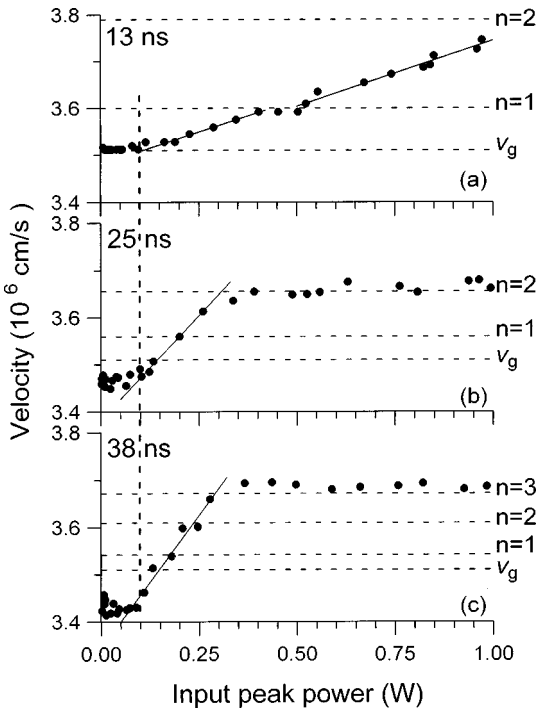

FIG. 6. Propagation velocity vs input peak power for MSBVW pulses propagated in the 7.56 μm-thick YIG film. For graphs (a), (b), and (c) the input pulse widths were 13, 25, and 38 ns, respectively. The carrier frequency was 5.00 GHz, the transducer separation was 6.1 mm, and the static magnetic field parallel to propagation direction was 1088 Oe. The horizontal dashed lines denote special velocities, as indicated. The vertical dashed line denotes the estimated threshold velocity for nonlinear response.

double the separation for the Fig. 5 data, while the pulse widths are the same. Linear fits to the regions of the data where the velocity is increasing yields slope of $(2.55 \pm 0.03)\times 10^5$ cm/s W and $(2.78\pm 0.04)\times 10^5$ cm/s W for Figs. 5 and 6(a), respectively. These results indicate that there is no significant difference in the velocity-power response for the same pulse width and a factor-of-2 change in transducer spacing.

The additional feature of these Fig. 5 and Fig. 6(a) data concerns the data points near the $n=1$ horizontal reference line. Both sets of measurements give an indication of a possible leveling off in the velocity response around this line. This effect is not particularly distinct for Figs. 5 and 6(a). It provides, nevertheless, an important indication of soliton effects. Graphs (b) and (c) in Fig. 6 show related but more pronounced leveling off features. These features are discussed below, and their theoretical implications are considered in the next section.

The main point of comparison between Figs. 5 and 6(a) is in the demonstration that the velocity response for a given pulse width is essentially independent of the transducer separation. The main point of comparison for the three graphs in Fig. 6 is to demonstrate that the input pulse width has a dramatic effect on the velocity response. There are three effects: (i) the velocity versus power response; (ii) the velocity saturation; (iii) the low power limit velocity.

Consider the velocity versus power response first. Linear best fits to the velocity vs power data between input powers of 0.1 and 1 W for (a) and between 0.1 and 0.3 W for (b) and (c) yield slopes of $(2.78\pm 0.04)\times 10^5$ cm/s W, $(8.88\pm 0.01)\times 10^5$ cm/s W. It is clear from these values that the input pulse width has a critical effect on the velocity response. Over the range of the available data, the response is nearly linear, with a slope of 3.4×10^{-5} cm/ns^2 W.

Turn now to the velocity saturation evident in Fig. 6. While graph (a) shows no saturation for the range of powers available, graphs (b) and (c) show that the MME pulse velocity saturates abruptly at 3.66×10^6 cm/s for 25 ns-wide pulses and 3.68×10^6 cm/s for 38 ns-wide pulses. While these saturation values are about the same, the different pulse widths lead to very different threshold velocities for different order solitons, as indicated by the horizontal dashed lines. The significance of these thresholds will be discussed in the next section. The main point for this discussion of the data alone is that the velocity saturation for different pulse widths appear (i) to be at about the same velocity values and (ii) to be related to different order soliton processes.

Consider, finally, the low power limit velocity change with input pulse width. As discussed above, the group velocity value for these experiments, 3.51×10^6 cm/s, is taken from the measurement for low power and short 13 ns pulse widths. By definition, therefore, this v_g value and the low power limit velocity for the data in (a) are the same. Graphs (b) and (c), however, show data that indicate low power limit velocity values that are *smaller* than v_g. These low power limit velocity shifts are an artifact of the low power deformation in the output pulse shape at low powers and the time-of-flight algorithm for the determination of t_c from Eq. (1). Note the pulse shapes in Figs. 3(a) and 4(a), for example. For both graphs, these low power profiles show a small peak that comes earlier in time than a larger peak. As the power is

increased, the small and large peaks first change places, and then the small peak evolves to exhibit the multsoliton character discussed above.

IV. DISCUSSION

The results presented above reveal an important, new, and heretofore undiscovered MME soliton property, a power-dependent soliton velocity that exhibits distinct plateaus and saturation effects. The effect is small, on the order of five percent. The quantitative observation of these effects depends, to some extent, on a careful and self-consistent definition of pulse position in time as contained in Eq. (1), for example.

The purpose of this section is threefold: (a) To examine problems that are posed for this experimental effect in terms of the usual theory that is used to analyze MME soliton properties, based on the nonlinear Schrödinger (NLS) equation; (b) To consider some recently published theoretical results by Slavin[7] that connect soliton formation thresholds with modulational instability, and which may explain the observed saturation velocities; (c) To consider experimental correlations between the pulse profiles in Sec. III A and the soliton order indices inferred from Ref. 7.

A. Soliton solutions from the nonlinear Schrödinger equation

The propagation properties of MME wave packets may be analyzed on the basis of the NLS equation

$$i\left(\frac{\partial u}{\partial t}+\nu_g\frac{\partial u}{\partial z}+\eta u\right)+\frac{1}{2}D\frac{\partial^2 u}{\partial z^2}-N|u|^2u=0. \tag{2}$$

The parameter u corresponds to a scalar normalized complex one-dimensional envelope function $u(z,t)$ that represents the dynamic microwave magnetization response. The parameter z defines the propagation axis and t represents propagation time. The parameters ν_g and D denote the low power wave packet group velocity and the MSW dispersion coefficient, respectively, as defined above. The parameter η denotes the relaxation rate. A low amplitude plane-wave MSW signal would decay according to $u\propto e^{-\eta t}$. The parameter N is a nonlinear frequency shift coefficient defined as the change in the MSW frequency with the square of the modulus of u. The nomenclature for Eq. (2) and the above parameters is discussed in Ref. 3, among others.

For the case of zero relaxation or $\eta=0$, one may obtain an exact, analytical single soliton solution to Eq. (2) in the form[8,9]

$$u(z,t)=|u(z,t)|e^{i(\kappa_s z-\Omega_s t)}. \tag{3}$$

The amplitude $|u(z,t)|$ is given by

$$|u(z,t)|=u_0\ \mathrm{sech}\left[u_0\sqrt{\left|\frac{N}{D}\right|}(z-\nu_s t)\right]. \tag{4}$$

The frequency shift parameter Ω_s is given by

$$\Omega_s=\nu_g\kappa_s+\frac{1}{2}(D\kappa_s^2+Nu_0^2). \tag{5}$$

The wave packet or soliton velocity ν_s for the above solution is given by

$$\nu_s=\nu_g+\kappa_s D. \tag{6}$$

For the above solution, there are two free parameters, the soliton amplitude u_0 and the wave number parameter κ_s. Note that the complex exponential term in Eq. (3) does *not* represent the carrier signal for this nonlinear MME wave packet. The function $u(z,t)$ is *already* the envelope of the wave packet. The $i(\kappa_s z-\Omega_s t)$ term represents the additional phase which is added to the carrier phase term for the overall complex wave packet signal.

For the purposes of this work, the important property of the above solution is that the soliton velocity ν_s is independent of the soliton amplitude u_0. This velocity, while constant, need not be the same as the group velocity ν_g for a linear wave packet. That is, ν_s may differ from ν_g through the free parameter κ_s in accordance with Eq. (6). It should also be noted that Eqs. (3)–(6) are only for a single peaked order one envelope soliton. In a strict sense, therefore, the above NLS equation solution is applicable only to the data presented in Fig. 2, where one sees a profile that consists of a single peak.

For the purposes of this section, however, Eq. (6) will be taken as the operational equation for the soliton velocity, regardless of the soliton order. Subject to this assumption, the results from Figs. 5 and 6 may be used to obtain an empirical indication of the power-dependent behavior of κ_s, and hence, the soliton velocity. The data in Figs. 5 and 6 establish four empirical facts. First, it is clear the soliton wave-number parameter κ_s is a function of the input power and, hence, on the amplitude u_0. Second, the data indicate that the size of the $\kappa_s D$ term in Eq. (6) is on the order of 5% of ν_g. Third, the effect of the input pulse width on the velocity change with power, as shown in Fig. 6, suggests that κ_s is an inverse function of the pulse width. Fourth, the clear velocity saturation effects noted in Fig. 6 indicate that κ_s takes on discrete values.

The theoretical dilemma, therefore, may be stated as follows: On what physical basis may the soliton velocity, defined in terms of the soliton wave-number parameter κ_s, be assigned dependences on input power, pulse width, etc., which are consistent with the results of the experiments?

B. Discrete soliton wave-number parameters and soliton velocity

A recently published theoretical analysis by Slavin[7] on thresholds for envelope soliton formation speaks directly to the question posed above. This analysis is based on the observed similarity between the threshold condition for the formation of an order n soliton from a rectangular input pulse of duration time T, and the threshold condition for modulational instability of a spin-wave excitation in a nonlinear dispersion medium. A comparison of these related but distinctly different processes leads to a prescription that gives discrete values of the solition wave-number parameter κ and that corresponds to the threshold conditions for solitons of order $n=1$, 2, 3, etc. If these discrete κ values are used in

Eq. (6), the resulting velocity values closely match the velocity plateaus apparent from the experimental data of Sec. III.

The input pulse threshold amplitude u_n^{th} for the formation of an nth order envelope soliton from a rectangular input pulse of width T in the medium where the Lighthill criterion $ND<0$ is satisfied, may be obtained from the inverse scattering formalism.[8] In the limit of zero damping $\eta=0$, this threshold amplitude may be written as

$$u_n^{\text{th}}=\frac{1}{2}\sqrt{\left|\frac{D}{N}\right|}\left(\frac{(2n-1)\pi}{\nu_g T}\right). \tag{7}$$

A nonlinear propagating plane-wave magnetic excitation in the same medium will have a threshold amplitude for modulational instability. Let $u_{\text{mod}}^{\text{th}}$ denote the threshold at which such a wave becomes unstable to a modulational perturbation with the modulation wave number κ_{mod}. From Ref. 7, this threshold may be written as

$$u_{\text{mod}}^{\text{th}}=\frac{1}{2}\sqrt{\left|\frac{D}{N}\right|}\kappa_{\text{mod}}. \tag{8}$$

As noted in Ref. 7, the forms of the threshold expressions in Eqs. (7) and (8) are quite similar. If one assumes that the process of envelope soliton formation from a rectangular input wave packet is analogous to the process of modulational instability for a nonlinear plane wave, then the quality in the square bracket in Eq. (7) can be interpreted as a soliton wave-number parameter, analogous to κ_{mod}.

If one equates the thresholds in Eqs. (7) and (8), one obtains a simple expression for the wave-number parameter κ_{mod} applicable to an order n soliton. Let this wave-number parameter be denoted as $\kappa_s^{(n)}$. The result is

$$\kappa_s^{(n)}=\frac{(2n-1)\pi}{v_g T}. \tag{9}$$

Note that the n-dependent threshold amplitude for soliton formation leads directly to an n-dependent effective wave-number parameter for solitons as well. Substitution of Eq. (9) into Eq. (6) yields a simple prescription for the n-dependent soliton velocity $\nu_s^{(n)}$,

$$\nu_s^{(n)}=\nu_g+\frac{(2n-1)\pi D}{\nu_g T}. \tag{10}$$

Equation (10) provides a simple working equation for the velocity associated with a soliton of order n. It is to be emphasized that this equation does not derive from theory, but only from a comparison of the thresholds for soliton formation and for modulational instability. However, it is also to be noted that (1) this working equation is consistent with the four empirical points listed above, and (2) there are no adjustable parameters. These connections will be considered in more detail shortly.

Based on the above analysis and the result of Eq. (10), the significance of the horizontal dashed lines in Figs. 5 and 6 labeled $n=1$, $n=2$, and $n=3$ are now clear. These lines represent the values of the $\nu_s^{(n)}$ velocity values expected for $n=1$, $n=2$, and $n=3$ solitons, respectively.

First consider the results in Fig. 5 for a 13 ns input pulse width. In this case, the calculated first- and second-order soliton velocities from Eq. (10) are 3.60×10^6 cm/s and 3.79×10^6 cm/s, respectively. As pointed out in Sec. III B, the measured pulse velocities as a function of input peak power show a slight leveling off at an input peak power of 0.5 W and precisely at the velocity corresponding to $\nu_s^{(1)}$ from Eq. (10). As will be discussed shortly, this power level is significant. It corresponds to the power level for which an order one soliton is completely formed at the position of the output transducer. As the input power is further increased, the measured velocity continues to increase but does not reach the second dashed line at $\nu_s^{(2)}$.

The velocity saturation effects and the correlation between experiment and theory are even more clear in Fig. 6. Keep in mind that the main difference between Figs. 5 and 6 is in the separation between transducers, 3 mm for Fig. 5 and 6.1 mm for Fig. 6. As discussed in Ref. 5, the longer propagation distance provides better access to the properties of completely formed solitons.

The results in Fig. 6(a) for 13 ns input pulse width are essentially the same as just discussed. For Fig. 6(b), the calculated $\nu_s^{(1)}$ and $v_s^{(2)}$ values for $n=1$ and $n=2$ are 3.56×10^6 cm/s and 3.66×10^6 cm/s, respectively. Here, however, the wider input pulse width of 25 ns leads to a clear saturation in the measured soliton velocity. As the data and the $n=2$ dashed line in Fig. 6(b) show, this saturation occurs precisely at $\nu_s^{(2)}$. Again, it is to be emphasized that the $\nu_s^{(n)}$ values for the dashed lines are obtained with no adjustable parameters. For Fig. 6(c), the calculated $\nu_s^{(1)}$, $\nu_s^{(2)}$, and $\nu_s^{(2)}$ values for $n=1$, $n=2$, and $n=2$ are 3.54×10^6 cm/s, 3.61×10^6 cm/s, and 3.67×10^6 cm/s, respectively. Here, the input pulse width is 38 ns. This extremely wide input width leads to an experimental soliton saturation velocity at $\nu_s^{(3)}$. The above results demonstrate the correlation between the observed saturation velocities of nonlinear soliton wave packets obtained through the data and the time-of-flight algorithm of Eq. (1) and an ad hoc theoretical prediction for velocities of nth order envelope solitons given by Eq. (10).

In addition to the above, it is important to specify clearly what is *not* explained by the above considerations. First, the simple soliton-modulational instability connection does *nothing* to model the observed increase in velocity with power. In these transition power intervals, the velocity of the propagating nonlinear wave packet increases more-or-less linearly with input power, and the slope of this increase is larger for wider input pulse width T. Presently, there is no theory to explain the wave packet velocity in these intervals. Second, the time-of-flight approach to soliton velocity ignores the multipeaked nature of the actual pulse profiles evident in Figs. 3 and 4 for the higher power levels. The connection between multipeaked profiles and higher-order solitons has been considered in detail in Ref. 4. The connections presented above simply extend these considerations to velocity saturation.

V. CONCLUSION

The evolution of pulse shape and propagation time for MSBVW nonlinear wave packets excited by rectangular in-

put pulses of peak power P_{in} and with T in YIG films have been studied as a function of peak power of the input pulse. Through a time-of-flight analysis, propagation time has been converted to a group velocity of a nonlinear wave packet, and this power-dependent group velocity is found to have a number of important properties. First, the effect of power on the group velocity is found to be small, but significant. For the powers available experimentally, which extend well above the threshold power of first-order soliton formation, the velocities are found to increase with power by about 5%. Second, one obtains a direct correlation between the number of peaks associated with a given output pulse at a given power, the soliton order, and an experimentally observed saturation velocity. Third, the measured saturation velocities of MME solitons are found to match values obtained from a prescription based on predicted wave numbers for modulational instability and connections with the single soliton solution to the NLS equation.

ACKNOWLEDGMENTS

This work was supported by the National Science Foundation, Grant Nos. DMR-9400276 and DMR-9701640, the U.S. Army Research Office, Grant No. DAAHO4-95-1-0325, a Cottrell College Science Award from the Research Corporation, Grant No. CC-3401, and the Oakland University Foundation. H. X. acknowledges partial support by the National Science Foundation of China, and P. Kabos acknowledges partial support by the National Science Foundation of Slovakia. The YIG film sample was provided by Dr. J. D. Adam, Northrop-Grumman Science and Technology Center, Pittsburgh, Pennsylvania.

*On leave from the National Laboratory of Solid State Microstructures, Nanjing University, Nanjing 210093, China.

†On leave from the Slovak Institute of Technology, Bratislava, Slovakia.

[1] B. A. Kalinikos, N. G. Kovshikov, and A. N. Slavin, JETP Lett. **38**, 413 (1983).

[2] P. De Gasperis, R. Marcelli, and G. Miccoli, Phys. Rev. Lett. **59**, 481 (1987).

[3] M. Chen, M. A. Tsankov, J. M. Nash, and C. E. Patton, Phys. Rev. B **49**, 12 773 (1994).

[4] M. Nash, C. E. Patton, and P. Kabos, Phys. Rev. B **51**, 15 079 (1995).

[5] N. G. Kovshikov, B. A. Kalinikos, C. E. Patton, E. S. Wright, and J. M. Nash, Phys. Rev. B **54**, 15 210 (1996).

[6] H. Xia, P. Kabos, C. E. Patton, and H. E. Ensle, Phys. Rev. B **55**, 15 018 (1997).

[7] A. N. Slavin, Phys. Rev. Lett. **77**, 4644 (1996).

[8] V. E. Zakharov and A. B. Shabat, Sov. Phys. JETP **34**, 62 (1972).

[9] A. Hasegawa and F. Tappert, Appl. Phys. Lett. **23**, 142 (1973).